ORIGINAL RESEARCH PAPER

Check for updates

Facile engineering of aptamer-coupled silk fibroin encapsulated myogenic gold nanocomposites: investigation of antiproliferative activity and apoptosis induction

Poorni Kaliyappan Elayappan · Kavitha Kandasamy · Vadivukkarasi Sasikumar · Muruganantham Bharathi · Abdurahman Hajinur Hirad · Abdullah A. Alarfaj · Palanisamy Arulselvan · Ravindran Jaganathan · Rajeswari Ravindran · Jagadeesh Suriyaprakash · Indumathi Thangavelu

Abstract Nanocomposites selectively induce cancer cell death, holding potential for precise liver cancer treatment breakthroughs. This study assessed the cytotoxicity of gold nanocomposites (Au NCs) enclosed within silk fibroin (SF), aptamer (Ap), and the myogenic *Talaromyces purpureogenus* (TP) against a human liver cancer cell (HepG2). The ultimate product, Ap-SF-TP@Au NCs, results from a three-step process. This process involves the myogenic synthesis of TP@Au NCs derived from TP mycelial extract, encapsulation of SF on TP@Au NCs (SF-TP@Au NCs), and the conjugation of Ap within SF-TP@Au NCs. The synthesized NCs are analyzed by various characteristic techniques. Ap-SF-TP@Au NCs induced potential cell death in HepG2 cells but exhibited no cytotoxicity in non-cancerous cells (NIH3T3). The morphological changes in cells were examined through various biochemical staining methods. Thus, Ap-SF-TP@Au NCs emerge as a promising nanocomposite for treating diverse cancer cells.

Keywords Apoptosis · Aptamer, gold nanocomposites · Liver cancer · Silk fibroin

P. K. Elayappan · K. Kandasamy
Department of Biochemistry, Vivekanandha College of Arts and Sciences for Women (Autonomous), Elayampalayam, Tiruchengode, Namakkal, Tamil Nadu 637205, India

V. Sasikumar
Department of Biochemistry, K.S.Rangasamy College of Arts and Science, Tiruchengode, Namakkal, Tamil Nadu 637215, India

M. Bharathi
Center for Bioinformatics, Department of Biochemistry, Karpagam Academy of Higher Education, Coimbatore, Tamil Nadu 641021, India

A. H. Hirad · A. A. Alarfaj
Department of Botany and Microbiology, College of Science, King Saud University, P. O. Box. 2455, 11451 Riyadh, Saudi Arabia

P. Arulselvan
Department of Chemistry, Saveetha School of Engineering, Saveetha Institute of Medical and Technical Sciences (SIMATS), Saveetha University, Chennai, Tamil Nadu 602 105, India

R. Jaganathan · R. Ravindran
Preclinical Department, Faculty of Medicine, Universiti Kuala Lumpur, Royal College of Medicine Perak (UniKL-RCMP), 30450 Ipoh, Perak, Malaysia

J. Suriyaprakash
Guangdong Provincial Key Laboratory of Nanophotonic Functional Materials and Devices, School of Information and Optoelectronic Science and Engineering, South China Normal University, Guangzhou 510006, China

I. Thangavelu (✉)
Department of Chemistry, CHRIST (Deemed to Be University), Bangalore 560029, India
e-mail: indumathi.t@christuniversity.in

⚙ Springer

Introduction

Liver cancer stands as the leading global cause of mortality (Anwanwan et al. 2020), with a 100% fatality rate within a year, underscoring its profound medical significance (Wang et al. 2019). Most instances of liver cancer are identified at an advanced stage, necessitating intrusive procedures as the only recourse for potential cure, yielding a survival rate ranging from 10 to 30% (Kudo et al. 2020). Despite notable progress in treatment modalities such as surgery, chemotherapy, and radiotherapy, the ability to eliminate malignant cells remains relatively limited, and survival rates show marginal improvement (Calderaro et al. 2019). Hence, there is an urgent need for innovative screening, diagnostic, and therapeutic tools.

Nanotechnology has emerged as a promising solution to the significant drawbacks associated with current cancer treatments, such as chemotherapy and radiation therapy (Madamsetty et al. 2019; Indumathi et al. 2024). These traditional methods often lead to systemic toxicity, damage to healthy tissues, and limited efficacy against certain cancer types (Marques et al. 2020; Yeom et al. 2023; Aghebati-Maleki et al. 2020). Metal oxide nanoparticles, in particular, offer promise in anticancer treatment due to their unique properties (Madamsetty et al. 2019). They can be specifically tailored to target cancer cells, enhance drug delivery, and provide imaging capabilities, improving precision in treatment while minimizing harm to normal tissues. Additionally, certain metal oxide nanoparticles exhibit properties such as photothermal therapy and radiotherapy enhancement, further augmenting their therapeutic potential (Medici et al. 2021; Peng and Liang 2019). The biocompatibility and biodegradability of these nanoparticles, coupled with their capacity to act as carriers for therapeutic agents, make them attractive candidates for cancer treatment strategies. Despite these promising attributes, ongoing research is crucial to address safety concerns and ensure regulatory approval for their clinical use. The integration of metal oxide nanoparticles within the realm of nanotechnology holds the potential for more effective and targeted cancer therapies, marking a significant advancement in the field (Farzin et al. 2020).

Gold nanoparticles play a pivotal role in anticancer treatment due to their selective targeting ability, facilitating precise drug delivery with minimal impact on healthy cells (Goddard et al. 2020; Tian et al. 2022). These nanoparticles are adept at harnessing photothermal therapy (PTT), converting light into heat, and enabling localized cancer cell ablation. Functioning as drug carriers, gold nanoparticles ensure controlled release and enhanced drug bioavailability (Navyatha and Nara 2023; Ameen et al. 2023). Their unique optical properties make them valuable for imaging contrast in diagnostic techniques like computed tomography (CT) and photoacoustic imaging. However, the use of gold nanoparticles in biomedical applications raises concerns about potential toxicity and uncertainties regarding their long-term fate in the body. To overcome these challenges, the present research has explored encapsulating gold nanoparticles within SF, taking advantage of SF's biocompatibility and biodegradability. This encapsulation provides a protective shell, reducing direct interaction with biological systems and mitigating potential toxicity. The controlled degradation of SF allows for a gradual release of encapsulated gold nanoparticles, enhancing their safety profile. This innovative approach improves the suitability of gold nanoparticles for various biomedical applications, including myogenic applications, where considerations of biocompatibility and controlled release are paramount.

SF, synthesized in the silk glands of the Bombyx mori silkworm, constitutes specialized, high-molecular-weight proteins resembling block copolymers (Qian et al. 2020). Biotechnological applications involving SF proteins combined with colloidal Au NPs are viable (Ranjana et al. 2020; Hosseini et al. 2023; Ahmad et al. 2019). Even though native silk materials are quite strong and biocompatible, they aren't always up to snuff for some uses. The progress in physical, chemical, and genetic engineering in silks is modified and functionalized on multiple levels to attain specific qualities (Ahmad et al. 2019). One potential approach to obtaining silk derivatives and conjugation products with photosensitivity, cell attachment capacity, and anti-adhesion ability is chemically modifying the silk polymer chain via reactive amino acid groups. The delivery of anticancer drugs for cancer treatment has been the primary focus of research on tiny drug delivery from SF-based nanoparticles (Ranjana et al. 2020). Problems with biodistribution, systemic toxicity, and unwanted side effects plague the majority of today's anticancer drugs. Anticancer drugs must

reach the targeted tumor tissues via many pathways in the body while preserving as much of their therapeutic efficacy as possible outside the bloodstream (Dam et al. 2022; Khalifehzadeh and Arami 2020; Zhang et al. 2010; Some et al. 2020; Unal et al. 2020). Anticancer medicine can passively or actively target tumor cells, killing them off while sparing healthy cells from harm once they reach the tumor location. Also, for the drugs to work as intended, their release into the bloodstream needs to be carefully regulated. A promising new approach to cancer treatment has emerged with the creation of SF nanoparticles loaded with anticancer drugs. A lot of people are interested in SF nanoparticles that have anticancer drugs such as emodin, paclitaxel (PTX), curcumin, methotrexate, floxuridine, doxorubicin (DOX), and cis-dichlorodiamminoplatinum (Lakshmeesha Rao et al. 2017; Tunali et al. 2023).

The combination of Ap with SF encapsulation on gold nanoparticles presents a promising approach for anticancer drug delivery. Ap enables targeted delivery to cancer cells, minimizing off-target effects, while SF provides biocompatibility, biodegradability, and controlled drug release. The incorporation of gold nanoparticles enhances therapeutic effects and offers imaging capabilities. This synergistic system reduces potential toxicity concerns associated with bare nanoparticles, ensuring a safer and more effective anticancer drug delivery platform (Khorshid et al. 2023; Kar et al. 2023).

Endophytic fungi coexist within plant tissues without causing harm to the host. Myogenic NPs produced by endophytic fungi exhibit potential antioxidant, antibiotic, and anticancer effects (Akther et al. 2019; Munawer et al. 2020; Janakiraman et al. 2019). TP, an endophytic fungus residing in both marine and terrestrial plants, surpasses most endophytes in its ability to generate novel metabolites (such as butanamide, propanoic acid, phenol, urea, and pigment) and nanoparticles with anticancer, antibacterial, antioxidative, and antiproliferative properties (Akther et al. 2019; Munawer et al. 2020; Janakiraman et al. 2019). SF, owing to its low toxicity and biocompatibility, is employed in the creation of drug-delivery devices (Hu et al. 2019; Danagoudar et al. 2020; Clarance et al. 2020; Danagoudar et al. 2020). The present study aimed at myco-synthesis of gold nanocomposites utilizing TP. This study aimed to enhance cytotoxicity in human liver cancer cells by synthesizing TP@Au NCs through TP mycelial extract encapsulated in SF (SF-TP@Au NCs), followed by conjugation with an AP (Ap-SF-TP@Au NCs) (Fig. 1).

Materials and methods

Fabrication of TP@Au NCs using mycelial extract of TP

The fabrication of TP mycelial extracts followed established protocols as previously published (Mani
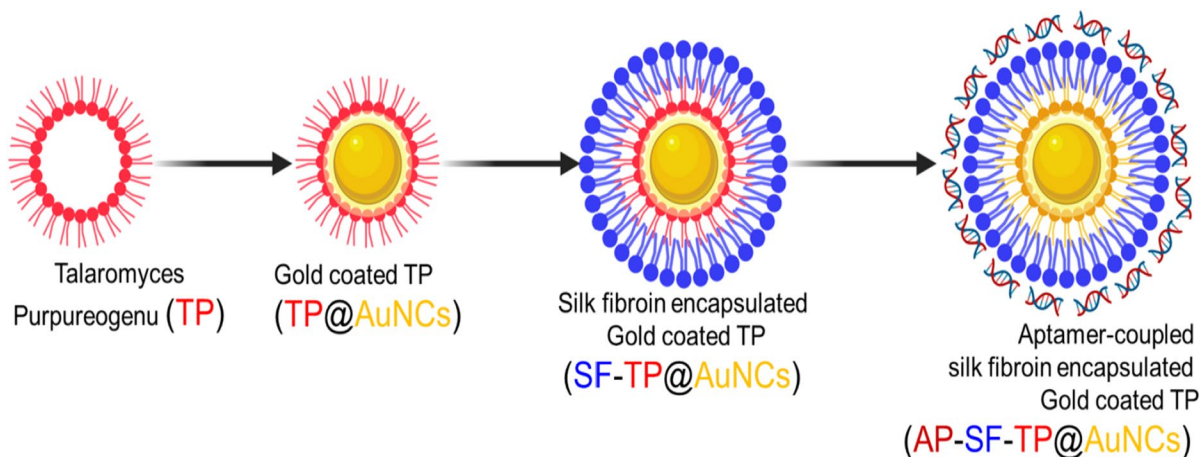
Fig. 1 The graphical representation of fabrication of aptamer-coupled silk fibroin encapsulated myogenic gold nanocomposites (Ap-SF-TP@AuNCs) for effective treatment of liver cancer

et al. 2021). In summary, 500 ml Erlenmeyer flasks were inoculated with 2 ml of fungal spore suspensions (7×10^7 spores/mL) and placed in a rotary shaker at 180 rpm at 27 °C for a week. After filtering the mycelial extract through the Whatman No.1 filter paper, it was collected. Subsequently, 25 ml of the mycelial extract was mixed with 100 ml of AuCl (10 mM) solution, and the mixture was placed in a shaking incubator at 29 °C, 180 rpm, in the dark for 72 h. To monitor the synthesis of TP@Au NCs, the UV–visible spectrum was utilized to document the gradual transformation of the solution's color from yellowish to pink and finally to dark purple. After centrifugation at 17,000 rpm to collect the TP@ Au NCs, the powder was lyophilized for subsequent experiments.

Preparation of SF solution

Aqueous SF solution was extracted from Bombyx mori cocoons using a well-established and effective method (Hu et al. 2019). In summary, 5 g of Bombyx mori cocoons underwent degumming in a Na_2CO_3 solution (0.02 M, 2 μL) at 100 °C for 0.5 h, followed by rinsing for 20 min in DI water with continuous stirring. Degummed silk was achieved after three processing rounds. To further process the degummed silk, it was immersed in a LiBr solution (9.3 mol/L, w/v = 15:100) at 60 °C for 4 h with continuous stirring. The subsequent step involved a 72-h room-temperature dialysis against DI water to eliminate the salt (14 kDa MW cutoff, Millipore). Ultrafiltration was employed to further concentrate the obtained SF solution to a concentration of 0.24 g/ml. Concentration measurement involved placing 1 ml of silk solution on a Petri plate and drying it to a constant weight in an oven set to 60 °C. A sample was considered to have maintained a constant weight if there was no more than a 0.1% shift in the weight percent of solids after 1 h of warming. Silk concentration was determined by subtracting the weight of the empty petri plate from the total weight of the dry silk and petri plate.

Encapsulation of SF on TP@Au NCs

A previously published technique for encapsulating TP@Au NCs in SF was adopted (Yu et al. 2023). In brief, 75 mg of SF was immersed in 20 ml of water and stirred at 90 rpm in a magnetic stirrer at room temperature for 12 h. On a subsequent day, 10 mg of TP@Au NCs was added to the SF solution, and the mixture underwent agitation for 30 min at 90 rpm before being sonicated for 10 min. A solution of 1.0 mg/ml of sodium triphosphate pentabasic was gently added to the TP@Au NCs-SF solutions, which were then stirred at 100 rpm at room temperature in the darkness for 24 h to create SF-TP@Au NCs. Centrifugation at 17,000 rpm for 15 min was then employed to extract the SF-TP@Au NCs.

Conjugation of Ap on SF-TP@Au NCs

Activation of covalent bonds in SF-TP@Au NCs via the EDC and NHS reaction facilitated the attachment of the DNA AP through conjugation. Specifically, SF-TP@Au NCs (2 ml, 1 mg/ml) were combined with EDC (25 μL, 0.1 mg/ml) and NHS (10 μl, 0.1 mg/ml), and the mixture was stored at 4 °C for 2 h. Subsequently, the SF-TP@Au NCs were incubated at 4 °C for a full 24 h after the addition of 30 μL of the AP solution. Following this, a dialysis membrane was employed to dialyze the Ap-SF-TP@Au NCs against deionized water at 4 °C for 12 h. Finally, the Ap-SF-TP@Au NCs were lyophilized into a single batch for use in subsequent research. Additionally, agarose gel electrophoresis confirmed AP conjugation with SF-TP@Au NCs (Abdussalam-Mohammed et al. 2023). The schematic diagram of the synthesis is given in Fig. 1.

In vitro release

To determine the number of TP@Au NCs released in vitro from Ap-SF-TP@Au NCs, diffusion through a dialysis membrane was employed. In brief, experiments on the release of pH-responsive nanocomposites utilized acetate buffer (pH 5.4) and phosphate buffer saline solution (pH 7.4) as representatives of varied pH solutions. The dialysis bag was loaded with a buffer solution containing Ap-SF-TP@Au NCs, diluted to 1 mg/ml, within a pH range of 7.4 to 5.4 (14 kDa). Subsequently, the dialysis bag was immersed in a 50 ml dissolving buffer (pH 5.4 and 7.4) at 37 °C with gentle stirring (100 rpm). Aliquots of the dissolution buffer were taken every 5 ml over an hour, and a UV spectrophotometer was utilized to

analyze them, determining the rate of nanocomposite release (Shahabadi et al. 2019).

Cell culture

Human liver cancer cells (HepG2) and mouse embryonic fibroblasts (NIH3T3) were cultured in high-glucose RPMI-1640 medium supplemented with 10% fetal bovine serum (FBS) and 1% penicillin–streptomycin at 37 °C in a humidified atmosphere with 5% CO_2. TP, TP@Au NCs, SF-TP@Au NCs, Ap-SF-TP@Au NCs, and cisplatin (100 mg/ml) in DMSO were prepared at different concentrations with RPMI 1640; in both control and treated cells, the final concentration of DMSO was less than 0.02%.

HepG2 and NIH3T3 cells were plated onto 96-well plates (5000 cells/well) and left overnight to form a semi-confluent monolayer. Cell monolayers were treated in quadrants with TP, TP@Au NCs, SF-TP@Au NCs, Ap-SF-TP@Au NCs, and cisplatin (0–2000 µg/ml) for an exposure time of 24 h. Subsequently, MTT solution in PBS (5 mg/ml) was added, and the formation of formazan crystals was visually confirmed. DMSO (100 µL/well) was added to dissolve the formazan crystals, after which the absorbance was read at 470 nm. Cell proliferation was assessed based on the optical density values and represented as a percentage relative to the control. IC_{50} values (the concentration of the sample causing 50% loss of cell proliferation compared to the vehicle control) were determined using non-linear regression curve fitting of the dose–response plots on GraphPad Prism V.8.0 software (Giriraj et al. 2022; Swaminathan et al. 2022; Kalaiarasi et al. 2022).

Apoptotic detection by fluorescence staining

The HepG2 cell density (1×10^5 cells) was cultured for 24 h. Following this period, the cells were treated with TP, TP@Au NCs, SF-TP@Au NCs, and Ap-SF-TP@Au NCs and kept for incubation. The control cells remained untreated. On a subsequent day, the IC_{50} concentration of the treated TP, TP@Au NCs, SF-TP@Au NCs, and Ap-SF-TP@Au NCs was mixed with acridine orange (AO) and ethidium bromide (EB) (5 mg/ml) on a coverslip (Mohamed Subarkhan et al. 2016; Sathiya Kamatchi et al. 2020; Mohan et al. 2018; Swaminathan et al. 2021). After a 5-min incubation, the cells were washed with PBS

thrice to remove unstained samples (at 5-min intervals) and photographed under a fluorescence microscope (Olympus microscopy-CKX53, Japan).

4′, 6-diamidino-2-phenylindole (DAPI) assay was conducted to recognize cell death. In brief, the HepG2 cell density (1×10^5cells) was cultured for 24 h. Following this period, the cells were treated with TP, TP@Au NCs, SF-TP@Au NCs, and Ap-SF-TP@Au NCs and kept for incubation. The control cells were left untreated. On the subsequent day, the IC_{50} concentration of the treated TP, TP@Au NCs, SF-TP@Au NCs, and Ap-SF-TP@Au NCs was mixed with DAPI dye (100 µL, 1 µg/ml) on a coverslip (Subarkhan et al. 2016; Wang et al. 2020; Mohamed Kasim et al. 2018). After a 5-min incubation, the cells were washed with PBS thrice to remove unstained samples (at 5-min intervals) and photographed under a fluorescence microscope (Olympus microscopy-CKX53, Japan).

Results and discussion

Nanocomposites characterization

The analysis of the UV–visible spectrum provides insights into the composition, size, and structure of nanocomposites (Dykman and Khlebtsov 2012; Ganapathy et al. 2024). Au NCs exhibit a distinct absorbance band in the visible spectrum due to their localized surface plasmon resonance (LSPR). Smaller nanospheres typically display predominant absorption with peaks around 520 nm, while larger spheres scatter light more significantly, resulting in broader and more diffuse peaks. As their size increases, larger spheres scatter light, exhibiting larger optical cross-sections (Avellan et al. 2017; Rai et al. 2010; Diegoli et al. 2006). Changes in the nanocomposite shape may lead to an expected blue or red shift in the maximum absorption. This alteration in the size of the optical cross-section induces changes in refractive index and reflectivity. Color shifts from yellow to light pink (Fig. 2A) suggest that the nanocomposites' size may exceed 25 nm, and the shape may deviate from perfect spherical, indicative of the LSPR relationship of gold. Various endophytic fungi have demonstrated the production of Au NCs with a similar UV–Vis spectrum. Furthermore, the peak absorbance of SF-TP@Au NCs exhibited a slight red-shift compared to that

Fig. 2 Assessment of UV–Vis spectrophotometer. (**A**) Different time interval effects of fabrication of TP@AuNCs. (**B**) UV–Vis spectral investigation of mycelial extract TP, AuCl, TP@AuNCs, and SF-TP@ AuNCs
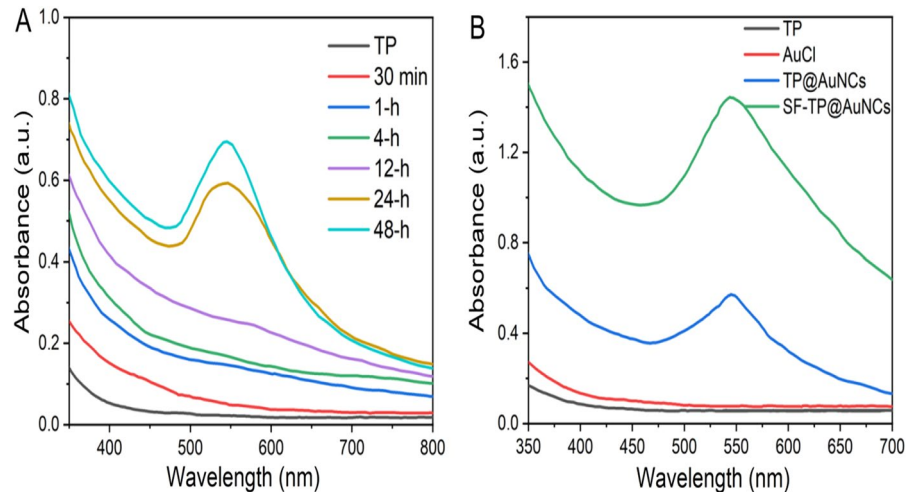

of TP@Au NCs (Fig. 2B), implying that the diameter of SF-TP@Au NCs is expected to be larger than that of TP@Au NCs, or the shape of SF-TP@Au NCs may differ from that of TP@Au NCs. The concentration of TPP, its absence, or the method of SF encapsulation may also play a role in the observed size variations (Elamin et al; 2023).

Dynamic Light Scattering (DLS) was employed to characterize SF-TP@Au NCs and TP@Au NCs for their diameter, polydispersity index (PDI), and δ-potential. The measurements indicated that TP@

Au NCs had a size of 57.24 ± 2.58 nm, while SF-TP@ Au NCs measured 92.48 ± 3.21 nm (Fig. 3A, B). The δ-potential, representing the charge on the particle's exterior, is crucial for stability and dispersion. TP@ Au NCs displayed a δ-potential of -59.48 ± 3.78 mV, while SF-TP@Au NCs exhibited a δ-potential of 46.79 ± 1.25 mV (Fig. 4A, B). The negative δ-potential of TP@Au NCs and the positive charge of SF-TP@Au NCs, as revealed by the zeta findings, indicate the stability conferred by the capping and encapsulating of SF and fungal metabolites. The

Fig. 3 Particle size measurements investigated by DLS. The fabricated myogenic gold nanocomposites (TP@AuNCs) and silk fibroin encapsulated (SF-TP@AuNCs) were prepared covalent bonding, and ionic gelation methods for the size were determined by DLS analysis
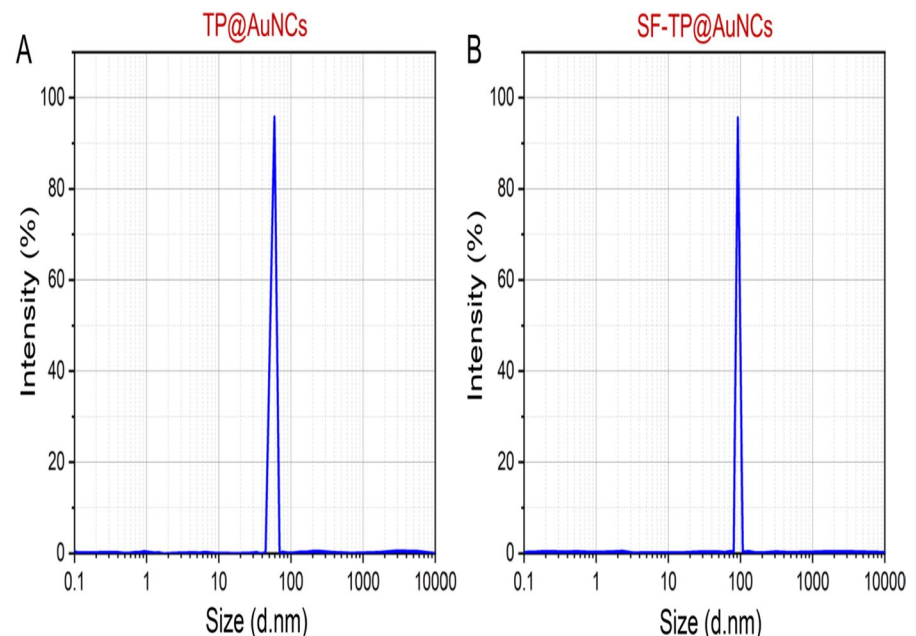
Fig. 4 Zeta potential sizes investigated by DLS. Myogenic gold nanocomposites (TP@AuNCs) and silk fibroin encapsulated (SF-TP@AuNCs) were prepared covalent bonding, and ionic gelation methods for the zeta potential were determined by DLS analysis
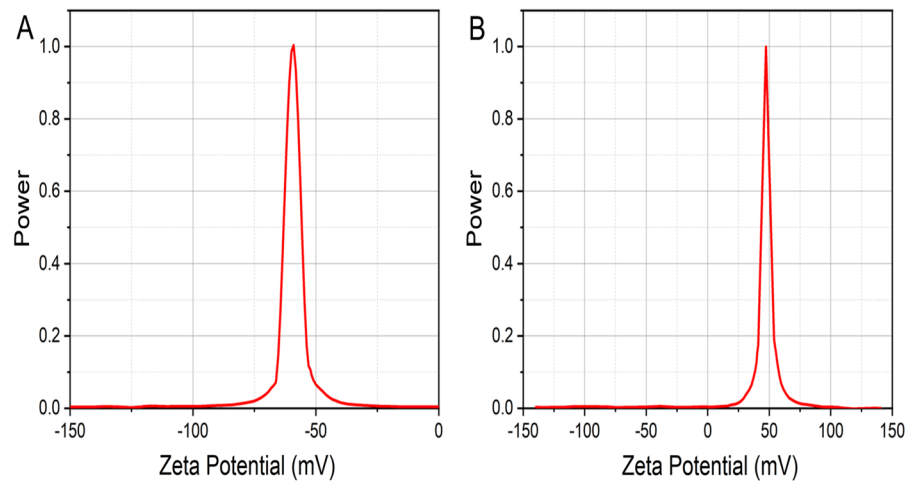

stability of the Ap-SF-TP@AuNCs was examined in particle diameter and polydispersity index (PDI) of the in water, PBS, and culture medium for 7 days. The particle diameter and polydispersity index (PDI) underwent no substantial changes in different conditions during the 7 days, which indicates the medical suitability of SF-TP@AuNCs (Fig. 5A, B).

Moreover, the X-ray diffraction (XRD) measurements confirmed the crystalline nature of both nanocomposites (Fig. 6A). In TP@Au NCs, peaks at (220), (200), and (111) with 2ө values of 66.24°, 45.44°, and 31.73°, respectively, were identified as signatures of TP@Au NCs. SF-TP@Au NCs displayed Bragg reflection peaks at (222), (311), (220), (200), and (111), with respective 2θ values of 83.98°, 75.27°, 56.48°, 45.48°, and 31.72° (Fig. 6B). Intense diffraction at 31.73° for TP@Au NCs and 45.48° for SF-TP@Au NCs indicated the growing size direction of zero-valent Au in the (111) directions for TP@Au NCs and the (200) direction for SF-TP@Au NCs. The distinctive XRD patterns of SF-TP@Au NCs and TP@Au NCs with different angle values confirm their differences in form and size.

Fourier transform infrared (FTIR) analysis was conducted to identify the molecular structures of TP, TP@Au NCs, and SF-TP@Au NCs (Fig. 7). The peaks at 1638 cm^{-1} and 2924 cm^{-1} in the TP extract were attributed to -C=C and -C-H alkanes stretching, and cyclic alkenes, respectively. These functional vibrations indicated the presence of phenolic chemicals in the TP extract. The remaining peaks at 1547 cm^{-1}, 1308 cm^{-1}, 1246 cm^{-1}, 1151 cm^{-1},

Fig. 5 Stability investigations of the Ap-SF-TP@AuNCs. (**A** and **B**) The stability of the Ap-SF-TP@AuNCs were examined in particle diameter, and polydispersity index (PDI) of the in water, PBS and culture medium for 7 days
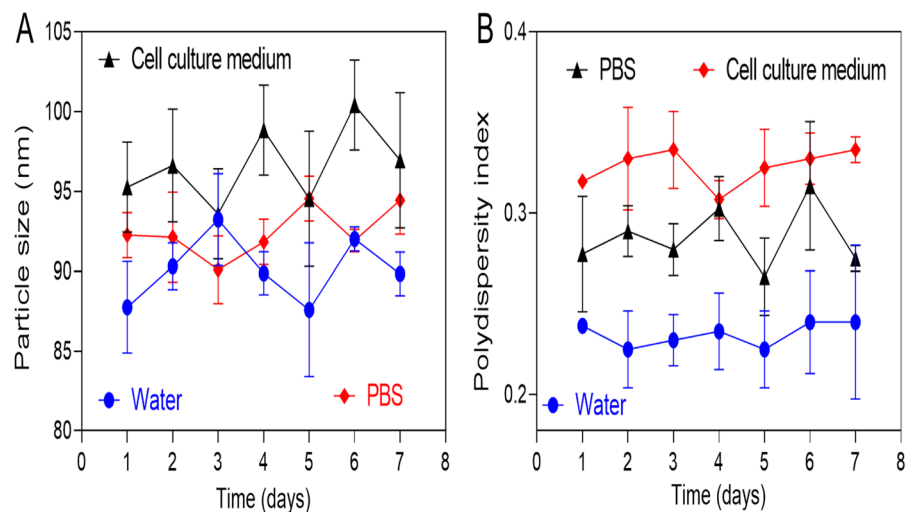
Fig. 6 The particle size and defects of Ap-SF-TP@ AuNCs were confirmed by the XRD pattern. XRD for fabricated (**A**) myogenic gold nanocomposites (TP@ AuNCs) and (**B**) silk fibroin encapsulated (SF-TP@ AuNCs)
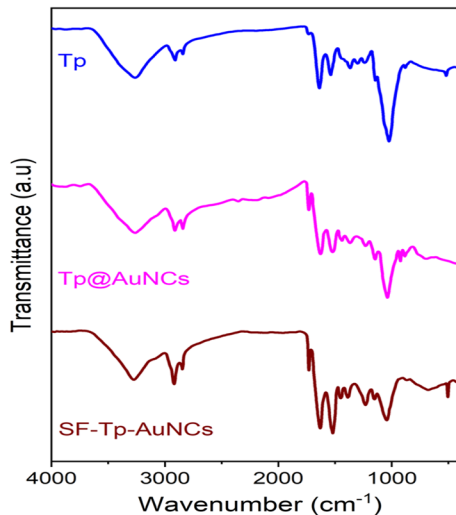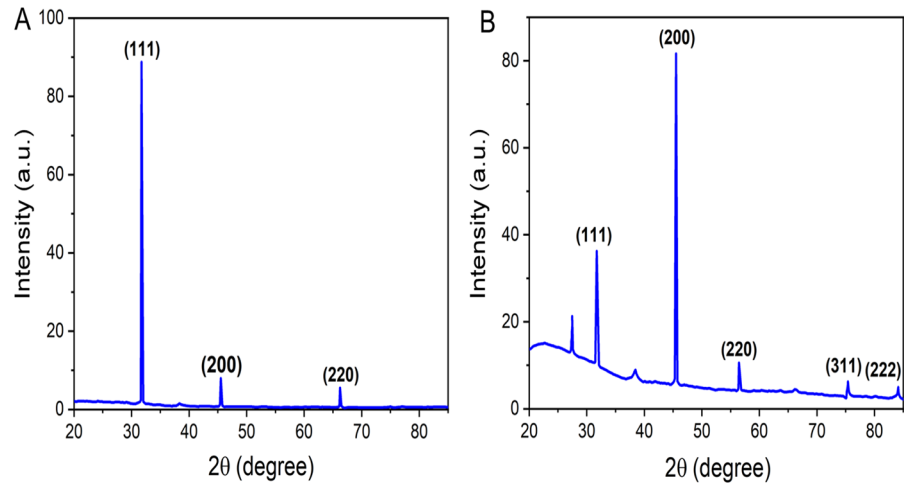

Fig. 7 FTIR investigated functional group shifts in TP, TP@ AuNCs, and SF-TP@AuNCs

and 1028 cm^{-1} were attributed to fungal metabolites such as pigment, terpenoids, and enzymes. In the spectra of TP@Au NCs, the peaks at 2919 cm^{-1}, 1451 cm^{-1}, and 1044 cm^{-1} were assigned to -C-N and -C-H stretching, respectively. These peaks were similar to those observed in the TP extract, confirming the capping of TP extracts on the surface of the nanoparticles. In SF-TP@Au NCs, significant peaks at 1741 cm^{-1} and 1631 cm^{-1} were observed, corresponding to -N–H and -C=O stretching of amide I and II in SF, respectively. The nitrogen-rich AP-functionalized surface of SF-TP@Au NCs did not result in noticeable changes in peaks. The verification of AP

conjugation in nanocomposites was consistent with previous studies that utilized agarose gel electrophoresis (saravanakumar et al. 2020).

Transmission electron microscopy (TEM) image illustrates the size and morphology of the nanocomposites (Fig. 8), both measuring less than 100 nm in size. Due to the inclusion of SF in their construction, SF-TP@Au NCs and Ap-SF-TP@Au NCs appeared larger than TP@Au NCs. TP@Au NCs exhibited spherical irregularities, while SF-Au NCs displayed a hexagonal crystal shape (Fig. 7). Variations in nanocomposite size and shape were attributed to the encapsulation of SF, cross-linked TP, and the pH of the nanocomposite solution. These TEM findings were consistent with the visible-light spectroscopy results. Ap-SF-TP@Au NCs exhibited a size and shape comparable to SF-TP@Au NCs (Fig. 8). It's important to note that TEM evaluates the nanocomposites directly, while DLS is performed on particles in an aqueous medium. TEM examination revealed a reduction in particle size, while DLS measures the hydrodynamic size of the particles. The pH-dependent release of the nanocomposites was also evaluated across a range of values (Fig. 9). Given the pH sensitivity of SF, the release of TP@Au NCs was notably more pronounced at pH 5.4 compared to pH 7.4. pH-sensitive drug release systems are designed to enhance drug delivery at specific locations in the human body where pH levels differ. In this context, the responsiveness of drug to a lower pH could be advantageous for targeted drug delivery, such as in environments associated with certain types of tumors or inflammatory conditions.
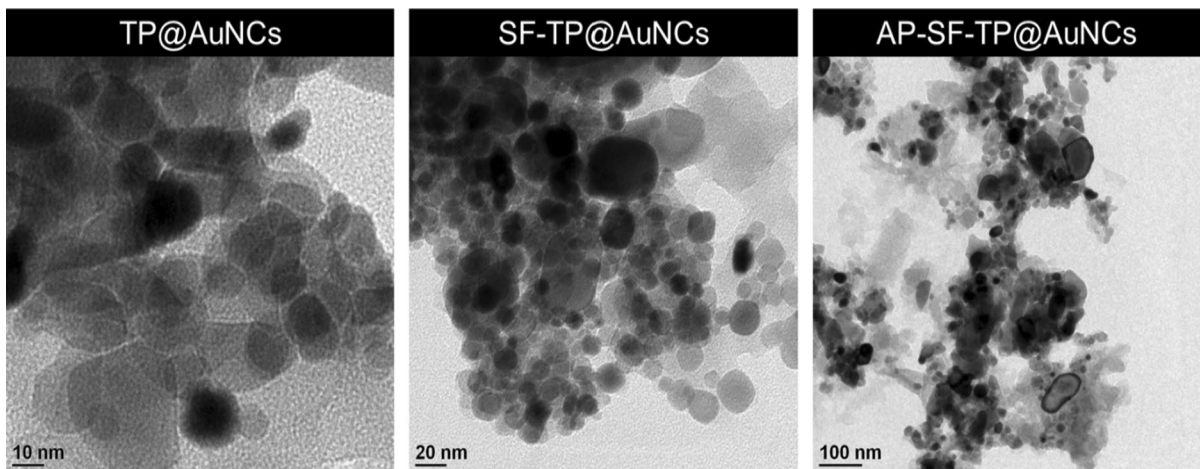
Fig. 8 Morphological shape of Ap-SF-TP@AuNCs confirmed by TEM analysis. TEM images of TP@AuNCs (scale bar 10 nm), SF-TP@AuNCs (scale bar 20 nm), and Ap-SF-TP@AuNCs (scale bar 100 nm)
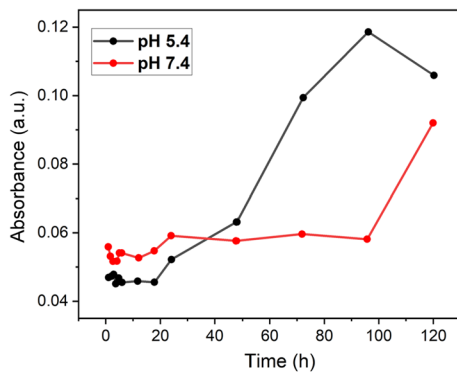
Fig. 9 In vitro drug release profile. TP-AuNCs release from the silk fibroin response to the different pH at various intervals

Cytotoxicity

The MTT assay was employed to assess the cytotoxicity of TP extract, TP@Au NCs, SF-TP@Au NCs, Ap-SF-TP@Au NCs, and cisplatin in mouse embryonic fibroblasts (NIH3T3) and human liver cancer cells (HepG2) (Fig. 10). All tested samples exhibited dose-dependent cytotoxicity in both NIH3T3 and HepG2 cells. TP and TP@Au NCs significantly reduced NIH3T3 cell viability, while SF-TP@Au NCs, Ap-SF-TP@Au NCs, and cisplatin did not (Fig. 10). The higher toxicity of TP and TP@Au NCs to NIH3T3 cells was attributed to fungal toxic chemicals. The lower cytotoxicity of SF-TP@

Au NCs and Ap-SF-TP@Au NCs in NIH3T3 cells was explained by their reduced internalization due to a lack of nucleolin expression and a slower pH decrease, resulting in less cytotoxicity and a lower pH-sensitive release of nanoparticles. In contrast, SF-TP@Au NCs and Ap-SF-TP@Au NCs demonstrated higher cytotoxicity in HepG2 cells compared to TP and TP@Au NCs, attributed to the acidic pH milieu and higher nucleolin expressions in cancer cells (Fig. 10).

Optical microscopic images depicting different viability concentrations are presented in Fig. 11, revealing morphological changes in NIH3T3 and HepG2 cell lines. The fabricated nanocomposites induced cell death in HepG2 cancer cells while sparing non-cancerous NIH3T3 cells. Ap-SF-TP@ Au NCs resulted in 60% cell death in HepG2 cells with no cytotoxicity towards NIH3T3 cells. The less cytotoxicity of fabricated Ap-SF-TP@AuNCs reveals high biocompatibility compared to cancer cells. These outcomes show the in vitro safety aspects of Ap-SF-TP@AuNCs. With remarkable biocompatibility, low cost, economic safety, water solubility, and surface bioactivity, the resulting Ap-SF-TP@AuNCs could be a promising drug candidate for anticancer agents. The targeted and pH-responsive release to nucleolin receptors made Ap-SF-TP@Au NCs the most effective anticancer agent among the samples.

Fig. 10 In vitro cytotoxicity of various samples assessed by MTT assay. NIH3T3 non-cancerous cells and HepG2 liver cancer cells subjected to the TP, TP@AuNCs, SF-TP@AuNCs, Ap-SF-TP@AuNCs and Cisplatin (commercial drug) in 24-h incubation
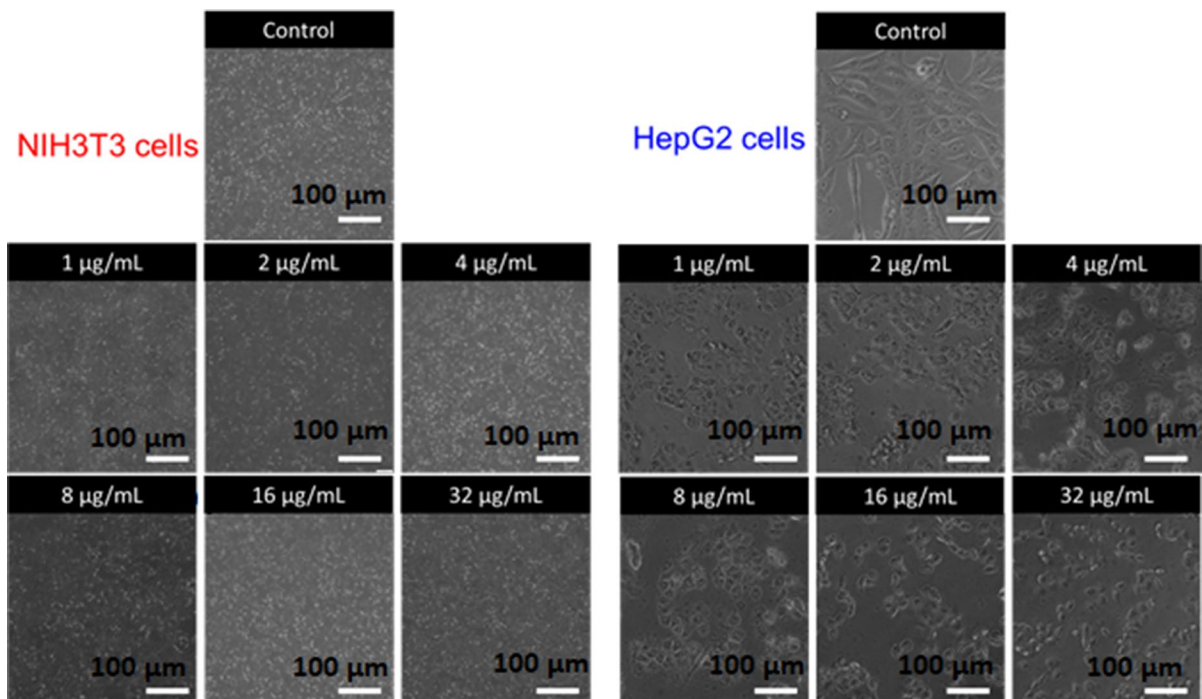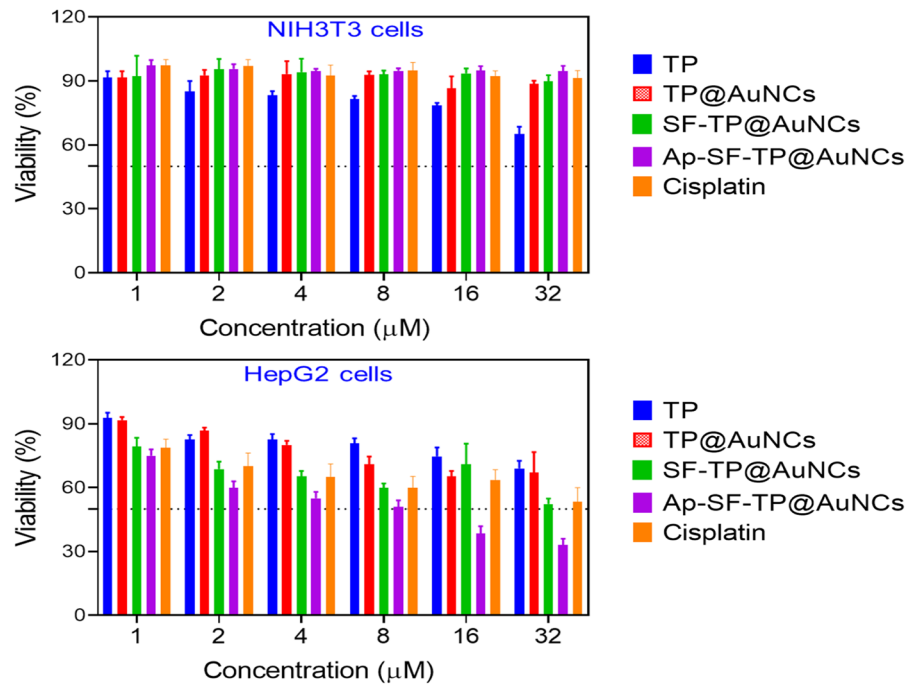
Fig. 11 Optical microscopic images of NIH3T3 non-cancerous cells and HepG2 liver cancer cells. Morphological changes of the NIH3T3 non-cancerous cells and HepG2 liver cancer cells with Ap-SF-TP@AuNCs in for 24-h

AO-EB dual staining assay

Anticancer drugs typically induce apoptosis in cancer cells (Zhao et al. 2019), making the investigation of apoptosis more crucial than relying solely on the standard MTT cell viability test, which does not distinguish between apoptotic and dead cells. The dual AO/EB assay is a fast, simple, and highly reliable method for detecting apoptosis. In Fig. 12, fluorescence images show control HepG2 cells and cells treated with TP, TP@Au NCs, SF-TP@Au NCs, and Ap-SF-TP@Au NCs at the IC_{50} concentration. DNA staining and examination of fluorescence microscopy images enable the discrimination between normal, apoptotic, and necrotic HepG2 cell morphology (Lakshmeesha Rao et al. 2017).

Under the microscope, healthy cells exhibit green fluorescence (Fig. 12), while apoptotic cells fluoresce orange due to nuclear blebbing and shrinkage. Necrotic cells appear red in fluorescence (Fig. 12) because the toxicity of TP, TP@Au NCs, SF-TP@Au NCs, and Ap-SF-TP@Au NCs has compromised their membranes. The AO-EB assay demonstrates that Ap-SF-TP@Au NCs at the IC_{50} concentration limit growth and induce apoptosis, as evidenced by the color transition from green to red. AO staining of normal, live cells with intact membranes results in green

fluorescence, while EB staining of damaged membranes results in orange/red fluorescence following the intercalation of both dyes. These findings align with those described by Hu et al. who found that the addition of aptamer and chitosan-encapsulated TP@Au NCs to liver cancer cells induced apoptosis characterized by nuclear fragmentation and cell membrane blebbing.
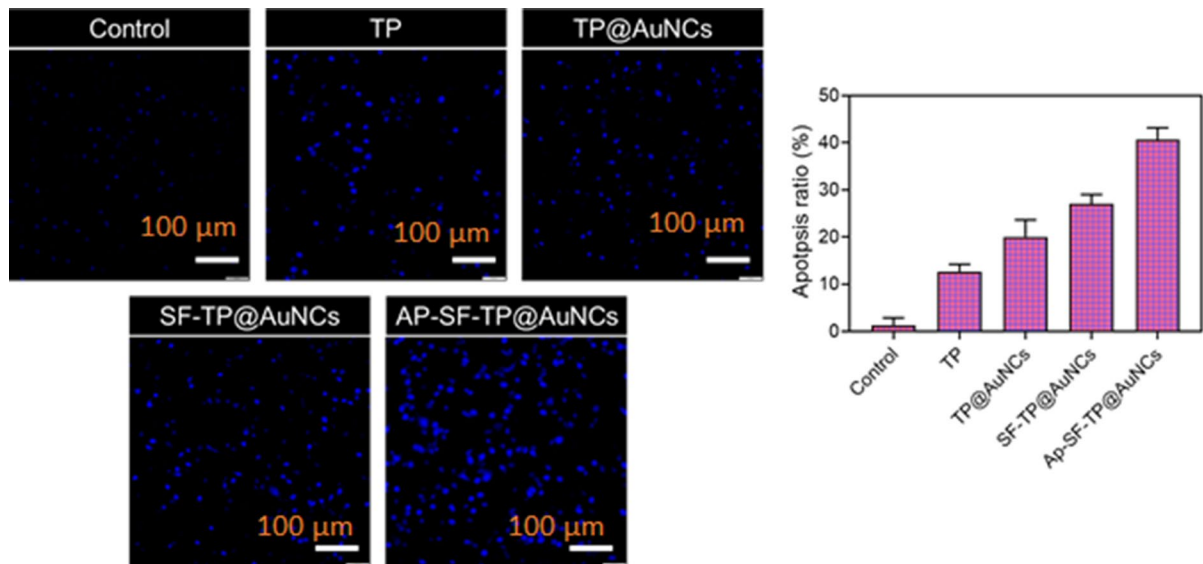
DAPI staining assay

DAPI, a nuclear fluorescent dye that strongly binds to DNA, was utilized to stain HepG2 cells and determine whether TP, TP@Au NCs, SF-TP@Au NCs, and Ap-SF-TP@Au NCs mediate cell death. Micrographs of DAPI staining in control and treated HepG2 cells at 24 h are presented in Fig. 13. When DAPI binds to DNA, it induces a bright blue fluorescence in the stained cells. In comparison to control cells, HepG2 cells treated with Ap-SF-TP@Au NCs exhibited a more intense blue fluorescence, indicating more condensed or fragmented chromatin (Fig. 13). These results indicated that Ap-SF-TP@Au NCs induced enhanced dose-dependent apoptosis in HepG2 cells. Additionally, HepG2 cells exposed to Ap-SF-TP@Au NCs lost their ability to attach, and their membranes appeared to degrade, suggesting that the particles
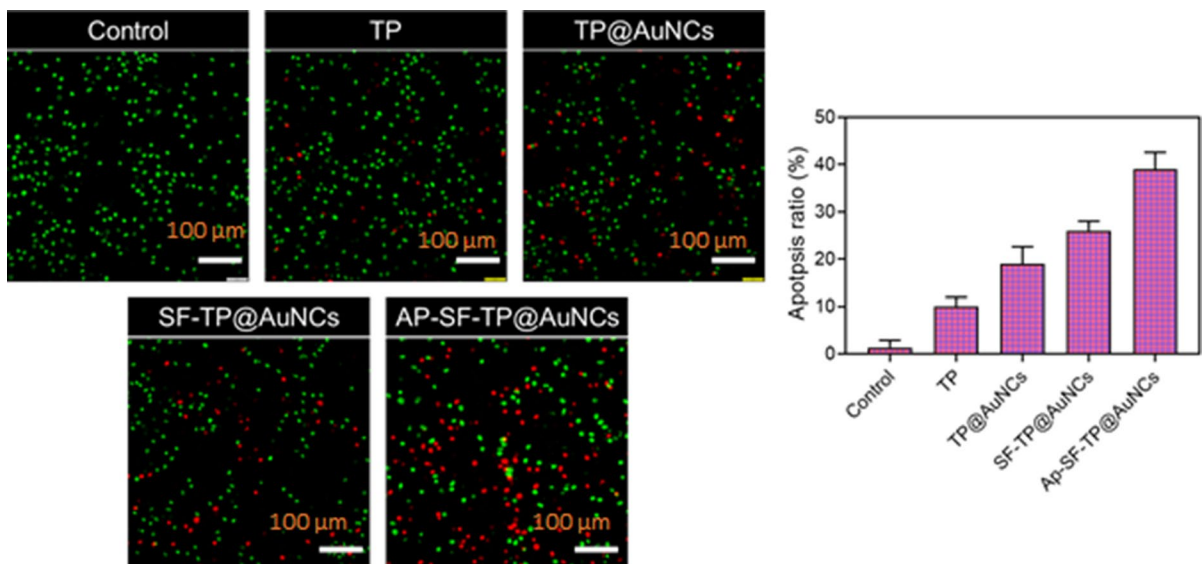
Fig. 12 Morphological changes investigated by AO-EB staining images were investigated by fluorescence microscope. HepG2 liver cancer cells subjected to the TP, TP@AuNCs, SF-TP@AuNCs, Ap-SF-TP@AuNCs for 24-h incubation. Respective apoptosis ratio of the fluorescence microscopy

Fig. 13 Nuclear damages were examined by DAPI staining images were investigated by fluorescence microscope. HepG2 liver cancer cells subjected to the TP, TP@AuNCs, SF-TP@ AuNCs, and Ap-SF-TP@AuNCs for 24-h incubation. Respective apoptosis ratio of the fluorescence microscopy

may dissolve cells by activating membrane-precipitating proteins.

The findings of this study suggest that Ap-SF-TP@Au NCs have anticancer potential for use in other procedures. Ap-SF-TP@Au NCs show promise as a potential drug for cancer treatment; nevertheless, these possibilities need thorough examination, and additional studies are necessary to address these complexities.

Conclusion

The cytotoxicity of liver cancer cells was enhanced by encapsulating SF and conjugating the AP with newly developed myogenic TP@Au NCs. Characterization data revealed that SF encapsulation significantly influenced the size and shape of TP@Au NCs. TP@Au NCs were spherical with a negative zeta charge, while Ap-SF-TP@Au NCs were hexagonal and positively charged. NIH3T3 cells were more sensitive to the cytotoxicity of TP@Au NCs compared to Ap-SF-TP@Au NCs. However, Ap-SF-TP@Au NCs exhibited greater cytotoxicity against HepG2 cells than control AP conjugates, likely due to the acidic pH of cancer cells. Additionally, Ap-SF-TP@Au NCs induced more cytotoxicity in

HepG2 cells by regulating ROS production and the expression of apoptosis-related proteins, as determined by various cell cytotoxicity assays. The cost advantages of Ap-SF-TP@AuNCs stem from an economical three-step synthesis process involving TP mycelial extract and SF, both known for their affordability. This method not only utilizes low-cost materials but also demonstrates potent cytotoxic activity against human liver cancer cells (HepG2), with no harm to non-cancerous cells. The efficient and selective cell death induction suggests that Ap-SF-TP@AuNCs may require lower concentrations for therapeutic effects, potentially reducing overall treatment costs. The use of sustainable sources, such as TP mycelial extract, further contributes to the cost-effectiveness of this nanocomposite, making it a promising and economically viable candidate for treating various cancer cells. In summary, further research on animals is needed to understand the chemical processes involved when using Ap-SF-TP@Au NCs.

Data availability Data sharing not applicable – no new data generated.

Declarations

References

Abdussalam-Mohammed W, Amar IA, AlMaky MM, Abdelhameed A, Errayes AO (2023) Silver nanoparticles and protein polymer-based nanomedicines. In: Protein-based biopolymers, pp 239–311. Woodhead Publishing

Aghebati-Maleki A, Dolati S, Ahmadi M, Baghbanzhadeh A, Asadi M, Fotouhi A et al (2020) Nanoparticles and cancer therapy: perspectives for application of nanoparticles in the treatment of cancers. J Cell Physiol 235(3):1962–1972

Ahmad A, Khan F, Mishra RK, Khan R (2019) Precision cancer nanotherapy: evolving role of multifunctional nanoparticles for cancer active targeting. J Med Chem 62(23):10475–10496

Akther T, Mathipi V, Kumar NS, Davoodbasha M, Srinivasan H (2019) Fungal-mediated synthesis of pharmaceutically active silver nanoparticles and anticancer property against A549 cells through apoptosis. Environ Sci Pollut Res 26:13649–13657

Ameen F, Al-Maary KS, Almansob A, AlNadhari S (2023) Antioxidant, antibacterial and anticancer efficacy of Alternaria chlamydospora-mediated gold nanoparticles. Appl Nanosci 13(3):2233–2240

Anwanwan D, Singh SK, Singh S, Saikam V, Singh R (2020) Challenges in liver cancer and possible treatment approaches. Biochimica et Biophysica Acta (BBA)-Rev Cancer 1873(1):188314

Avellan A, Schwab F, Masion A, Chaurand P, Borschneck D, Vidal V et al (2017) Nanoparticle uptake in plants: gold nanomaterial localized in roots of Arabidopsis thaliana by X-ray computed nanotomography and hyperspectral imaging. Environ Sci Technol 51(15):8682–8691

Calderaro J, Ziol M, Paradis V, Zucman-Rossi J (2019) Molecular and histological correlations in liver cancer. J Hepatol 71(3):616–630

Clarance P, Luvankar B, Sales J, Khusro A, Agastian P, Tack JC et al (2020) Green synthesis and characterization of gold nanoparticles using endophytic fungi Fusarium solani and its in-vitro anticancer and biomedical applications. Saudi Journal of Biological Sciences 27(2):706–712

Dam P, Altuntas S, Mondal R, Baudrit JRV, Kati A, Ghorai S et al (2022) Silk-based nano-biocomposite scaffolds for skin organogenesis. Mater Lett 327:133024

Danagoudar A, Pratap GK, Shantaram M, Ghosh K, Kanade SR, Joshi CG (2020) Characterization, cytotoxic and antioxidant potential of silver nanoparticles biosynthesised using endophytic fungus (Penicillium citrinum CGJ-C1). Materials Today Communications 25:101385

Diegoli S, Mendes PM, Baguley ER, Leigh SJ, Iqbal P, Garcia Diaz YR et al (2006) pH-Dependent gold nanoparticle self-organization on functionalized Si/SiO2 surfaces. J Exp Nanosci 1(3):333–353

Dykman L, Khlebtsov N (2012) Gold nanoparticles in biomedical applications: recent advances and perspectives. Chem Soc Rev 41(6):2256–2282

Elamin NY, Indumathi T, Kumar ER (2023) Pluronic f127 encapsulated titanium dioxide nanoparticles: evaluation of physiochemical properties for biological applications. J Mol Liq 379:121655

Farzin A, Etesami SA, Quint J, Memic A, Tamayol A (2020) Magnetic nanoparticles in cancer therapy and diagnosis. Adv Healthcare Mater 9(9):1901058

Ganapathy K, Rastogi V, Lora CP, Suriyaprakash J, Alarfaj AA, Hirad AH, Indumathi T (2024) Biogenic synthesis of dopamine/carboxymethyl cellulose/TiO2 nanoparticles using Psidium guajava leaf extract with enhanced antimicrobial and anticancer activities. Bioprocess Biosyst Eng 47(1):131–143

Giriraj K, Mohamed Kasim MS, Balasubramaniam K, Thangavel SK, Venkatesan J, Suresh S et al (2022) Various coordination modes of new coumarin Schiff bases toward Cobalt (III) ion: synthesis, spectral characterization, *in vitro* cytotoxic activity, and investigation of apoptosis. Appl Organomet Chem 36(3):e6536

Goddard ZR, Marín MJ, Russell DA, Searcey M (2020) Active targeting of gold nanoparticles as cancer therapeutics. Chem Soc Rev 49(23):8774–8789

Hosseini SA, Kardani A, Yaghoobi H (2023) A comprehensive review of cancer therapies mediated by conjugated gold nanoparticles with nucleic acid. Int J Biol Macromol 127184

Hu X, Saravanakumar K, Jin T, Wang MH (2019) Mycosynthesis, characterization, anticancer and antibacterial activity of silver nanoparticles from endophytic fungus Talaromyces purpureogenus. Int J Nanomed 9(14):3427–3438

Indumathi T, Kumaresan I, Suriyaprakash J, Alarfaj AA, Hirad AH, Jaganathan R, Mathanmohun M (2024) Synthesis and characterization of 4-nitro benzaldehyde with ZnO-based nanoparticles for biomedical applications. J Basic Microbiol 64(2):e2300494

Janakiraman V, Govindarajan K, Magesh CR (2019) Biosynthesis of silver nanoparticles from endophytic fungi, and its cytotoxic activity. Bionanoscience 9:573–579

Kalaiarasi G, Subarkhan MM, Safwana CF, Sruthi S, Kamatchi TS, Keerthana B, Kumar SA (2022) New organoruthenium (II) complexes containing N, X-donor (X= O, S) heterocyclic chelators: synthesis, spectral characterization, *in vitro* cytotoxicity and apoptosis investigation. Inorg Chim Acta 535:120863

Kar A, Rout SR, Giri L, Sahebkar A, Kesharwani P, Dandela R (2023) Aptamer-functionalized nanoparticles for targeted cancer therapy. In: Aptamers engineered nanocarriers for cancer therapy, pp 191–218. Woodhead Publishing

Kasim MSM, Sundar S, Rengan R (2018) Synthesis and structure of new binuclear ruthenium (II) arene benzil bis (benzoylhydrazone) complexes: investigation on antiproliferative activity and apoptosis induction. Inorganic Chem Front 5(3):585–596

Khalifehzadeh R, Arami H (2020) Biodegradable calcium phosphate nanoparticles for cancer therapy. Adv Coll Interface Sci 279:102157

Khorshid M, Varshosaz J, Rostami M, Haghiralsadat F, Akbari V, Khorshid P (2023) Anti HER-2 aptamer functionalized gold nanoparticles of dasatinib for targeted chemoradiotherapy in breast cancer cells. Biomaterials Adv 154:213591

Kudo M, Izumi N, Kubo S, Kokudo N, Sakamoto M, Shiina S et al (2020) Report of the 20th nationwide follow-up survey of primary liver cancer in Japan. Hepatol Res 50(1):15–46

Lakshmeesha Rao B, Gowda M, Asha S, Byrappa K, Narayana B, Somashekar R et al (2017) Rapid synthesis of gold nanoparticles using silk fibroin: characterization, antibacterial activity, and anticancer properties. Gold Bulletin 50:289–297

Madamsetty VS, Mukherjee A, Mukherjee S (2019) Recent trends of the bio-inspired nanoparticles in cancer theranostics. Front Pharmacol 10:1264

Mani VM, Kalaivani S, Sabarathinam S, Vasuki M, Soundari AJPG, Das MA et al (2021) Copper oxide nanoparticles synthesized from an endophytic fungus Aspergillus terreus: bioactivity and anti-cancer evaluations. Environ Res 201:111502

Marques AC, Costa PJ, Velho S, Amaral MH (2020) Functionalizing nanoparticles with cancer-targeting antibodies: a comparison of strategies. J Control Release 320:180–200

Medici S, Peana M, Coradduzza D, Zoroddu MA (2021, November) Gold nanoparticles and cancer: detection, diagnosis and therapy. In: Seminars in cancer biology, vol 76, pp 27–37. Academic Press

Mohan N, Subarkhan MKM, Ramesh R (2018) Synthesis, antiproliferative activity and apoptosis-promoting effects of arene ruthenium (II) complexes with N, O chelating ligands. J Organomet Chem 859:124–131

Munawer U, Raghavendra VB, Ningaraju S, Krishna KL, Ghosh AR, Melappa G, Pugazhendhi A (2020) Biofabrication of gold nanoparticles mediated by the endophytic Cladosporium species: photodegradation, in vitro anticancer activity and in vivo antitumor studies. Int J Pharm 588:119729

Navyatha B, Nara S (2023) Aptamer-and antibody-conjugated gold nanobipyramids—a study on cytotoxicity towards breast cancer cell lines. J Nanopart Res 25(8):165

Peng J, Liang X (2019) Progress in research on gold nanoparticles in cancer management. Medicine 98(18):e15311

Qian KY, Song Y, Yan X, Dong L, Xue J, Xu Y et al (2020) Injectable ferrimagnetic silk fibroin hydrogel for magnetic hyperthermia ablation of deep tumor. Biomaterials 259:120299

Rai A, Prabhune A, Perry CC (2010) Antibiotic mediated synthesis of gold nanoparticles with potent antimicrobial activity and their application in antimicrobial coatings. J Mater Chem 20(32):6789–6798

Ranjana R, Parushuram N, Harisha KS, Narayana B, Sangappa Y (2020) Photo-driven synthesis of anisotropic gold nanoparticles using silk fibroin—cell viability activities in lymphocyte and Jurkat cancer cells. BioNanoScience 10:864–875

Saravanakumar K, Sathiyaseelan A, Mariadoss AVA, Jeevithan E, Hu X, Shin S, Wang MH (2020) Dual stimuli-responsive release of aptamer AS1411 decorated erlotinib loaded chitosan nanoparticles for non-small-cell lung carcinoma therapy. Carbohyd Polym 245:116407

Sathiya Kamatchi TS, Subarkhan MKM, Ramesh R, Wang H, Małecki JG (2020) Investigation into antiproliferative activity and apoptosis mechanism of new arene Ru (ii) carbazole-based hydrazone complexes. Dalton Trans 49(32):11385–11395

Shahabadi N, Razlansari M, Zhaleh H, Mansouri K (2019) Antiproliferative effects of new magnetic pH-responsive drug delivery system composed of Fe3O4, CaAl layered double hydroxide and levodopa on melanoma cancer cells. Mater Sci Eng, C 101:472–486

Some S, Sarkar B, Biswas K, Jana TK, Bhattacharjya D, Dam P et al (2020) Bio-molecule functionalized rapid one-pot green synthesis of silver nanoparticles and their efficacy toward the multidrug resistant (MDR) gut bacteria of silkworms (Bombyx mori). RSC Adv 10(38):22742–22757

Subarkhan MKM, Ramesh R, Liu Y (2016) Synthesis and molecular structure of arene ruthenium (II) benzhydrazone complexes: impact of substitution at the chelating ligand and arene moiety on antiproliferative activity. New J Chem 40(11):9813–9823

Swaminathan S, Haribabu J, Subarkhan MKM, Gayathri D, Balakrishnan N, Bhuvanesh N et al (2021) Impact of aliphatic acyl and aromatic thioamide substituents on the anticancer activity of Ru (ii)-p-cymene complexes with acylthiourea ligands—in vitro and in vivo studies. Dalton Trans 50(44):16311–16325

Swaminathan S, Haribabu J, Mohamed Subarkhan MK, Manonmani G, Senthilkumar K, Balakrishnan N et al (2022) Coordination behavior of acylthiourea ligands in their Ru (II)–benzene complexes— structures and anticancer activity. Organometallics 41(13):1621–1630

Tian H, Zhang T, Qin S, Huang Z, Zhou L, Shi J et al (2022) Enhancing the therapeutic efficacy of nanoparticles for cancer treatment using versatile targeted strategies. J Hematol Oncol 15(1):1–40

Tunali BC, Akturk O, Sahingoz D, Turk M, Keskin AC (2023) Synthesis and characterization of polyethyleneimine/silk fibroin/gold nanoparticle nanocomposites: potential application as a gene carrier in breast cancer cell lines. Eur Polymer J 191:112042

Unal IS, Demirbas A, Onal I, Ildiz N, Ocsoy I (2020) One step preparation of stable gold nanoparticle using red cabbage extracts under UV light and its catalytic activity. J Photochem Photobiol, B 204:111800

Wang C, Vegna S, Jin H, Benedict B, Lieftink C, Ramirez C et al (2019) Inducing and exploiting vulnerabilities for the treatment of liver cancer. Nature 574(7777):268–272

Wang Y, Jin J, Shu L, Li T, Lu S, Subarkhan MKM et al (2020) New organometallic ruthenium (II) compounds synergistically show cytotoxic, antimetastatic and antiangiogenic activities for the treatment of metastatic cancer. Chem–A Eur J 26(66):15170–15182

Yeom JH, Shin E, Jin H, Liu H, Luo Y, Nam Y et al (2023) Aptamer-conjugated gold nanoparticles platform as the intracellular delivery of antibodies for cancer therapy. J Ind Eng Chem 126:480–491

Yu H, He M, Li Y, Liu Y, Xu Z, Zhang L et al (2023) A robust Au@ Cu2-xS nanoreactor assembled by silk fibroin for

enhanced intratumoral glucose depletion and redox dyshomeostasis. Biomaterials 293:121970

Zhang Y, Chen Y, Han D, Ocsoy I, Tan W (2010) Aptamers selected by cell-SELEX for application in cancer studies. Bioanalysis 2(5):907–918

Zhao Y, Zhao W, Lim YC, Liu T (2019) Salinomycin-loaded gold nanoparticles for treating cancer stem cells by ferroptosis-induced cell death. Mol Pharm 16(6):2532–2539